The Pennsylvania State University

The Graduate School

Department of Electrical Engineering

DIELECTRIC AND OPTICAL CHARACTERIZATION OF POLAR POLYMERIC MATERIALS: CHROMOPHORE ENTRAINED PMMA THIN FILMS

A Thesis in

Electrical Engineering

by

Kevin J. Deily

Submitted in Partial Fulfillment
of the Requirements
for the Degree of

Master of Science

August 2008

The thesis of Kevin J Deily was reviewed and approved* by the following:

Ruyan Guo
Professor of Electrical Engineering
Thesis Co-Advisor

Michael T Lanagan
Associate Professor of Engineering Science and Mechanics
Associate Director, Materials Research Institute
Thesis Co-Advisor

Joseph Dougherty
Associate Professor Emeritus of Material Science and Engineering
Thesis Co-Advisor

William Kenneth Jenkins
Professor of Electrical Engineering
Head of the Department of Electrical Engineering

*Signatures are on file in the Graduate School

ABSTRACT

The dielectric and optical response of thin film organic polymer poly(methyl methacrylate) (PMMA) doped with the chromophore *N*-Ethyl-*N*-(2-hydroxyethyl)-4-(4-nitrophenylazo)aniline (DR-1) samples were investigated over a wide frequency and temperature range for electro-optic. The DR-1 was directly doped into the PMMA matrix as a guest-host polymer system and three different concentrations of the DR-1 (0%, 5%, and 10% DR-1 by weight) were prepared. Thin film samples of uniform composition, thickness, and smoothness were successfully fabricated for all three concentrations by spin coating. The frequency and temperature dependent dielectric measurements were taken for the samples. The relative dielectric constant and loss factor were to be in good agreement with the reported values for the polymer system. A voltage was applied to the sample in an attempt to align the dipole moments of the chromophore. Breakdown in the film (the capacitance and loss shorting) was a problem with the thinner samples. A polarization verses electric field (P-E) measurement was taken and showed a weak nonlinear response that became more noticeable at elevated electric fields. Also, the biased dielectric measurement was determined by finding the slope of the linear section of the P-E graph. The index of refraction was determined using an ellipsometer. No observable electro-optic coefficient was measured from the samples using a Michelson electro-optic measurement configuration. It was determined that the current polymer samples were not ideal for electro-optic applications. A major contribution of the work was a methodology to extrapolate low frequency dielectric response to GHz and optical frequency.

TABLE OF CONTENTS

LIST OF FIGURES

LIST OF TABLES

ACKNOWLEDGEMENTS

I would like to thank my thesis committee Dr. Ruyan Guo, Dr. Michael Lanagan, Dr. Joe Dougherty, and Dr. Ken Jenkins, for all the help they have given me over the past two years with my research. Support for this project was provided by the Penn State Electro-Optics Center and Applied Research Laboratory. I would also like to thank Jason Claude and Brett Neese for providing me with information on the polymers; Guneet Sethi and Pratyush Tewari for helping with dielectric measurements; Jeff Long and Paul Moses for helping me use the various dielectric measurements setups; and Dr. John Fu and Dr. Hongbo Liu for helping with the optical setups and measurements. Finally, I would like to thank my friends and family. Without their support I surely would not be were I currently am in my life.

Chapter 1

Thesis Motivation

Polymeric organic materials have begun to receive more attention in the recent years due to the current developments in their application for high speed electro-optic (EO) devices. Most EO devices that are commercially available are made of an inorganic crystalline material (e.g. lithium niobate [$LiNbO_3$]). One of the major restrictions presently found with the inorganic EO devices are that their bandwidths usually cannot exceed 40 GHz without suffering severe performance loss [**1**]. This decrease in performance can be blamed on the higher dielectric constants and loss [**2**]. Another drawback of the current devices is the upper limits of the EO effect coefficients have already been reached (approximately 32 pm/V for $LiNbO_3$) [**3**]. Currently, polymer EO devices have been shown to generate much lower dielectric constants and loss, which help increase bandwidth. Certain polymer devices have been reported to have a bandwidth between 100 GHz and 300 GHz [**4**]. Furthermore, certain polymer systems have reported to have an EO effect coefficient ranging from 50 pm/V to 100 pm/V, which is two to three times larger than that of the $LiNbO_3$ device [**2**] [**5**]. In addition, polymeric materials in thin film form provide the advantages of large area, low operating voltage, and conforming in shape. Finally, crystalline based devices are much more difficult and expensive to fabricate when compared to polymer-based devices. This can be attributed to the time consuming and expensive method used to grow crystal, while a polymer can simply be mixed together using the proper components.

The major goal of this experiment was to investigate the possibility to synthesize efficient polymer sample that could take the place of the current mediums being used for EO devices. The assessment was conducted on the material level rather than on the device level. The main tasks of the thesis work are two fold: i) fabricating proper doped polymer thin film samples and ii) characterizing and measuring various properties of the prepared samples. This served as indicators for composition design and optimization of thin film fabrication. This was done by fabricating a number of polymer samples and testing their dielectric and optical properties. Once the testing was finished, it was determined if the polymer samples needed additional testing (in both fabrication dielectric and optical characterization) to determine if the polymer was a viable replacement.

Chapter 2

Introduction

Nonlinear Optics and Electro-Optic Effect

Nonlinear optics (NLO) is the study of the changes in optical properties of a material with the introduction of light. Lasers are typically used in NLO experiments given that they are a coherent probe for quantitative electro-optic effect measurement or they generate enough optical intensity to induce the nonlinear effects in most mediums [6]. When a beam strikes the material, it produces a change in the energy state of charges of the atoms. With the change of the charge, certain characteristics of the medium will be produced or altered (e.g. indices of refraction that phase, frequency, amplitude of the propagation waves, etc) [**3**]. One of the commonly measured properties of NLO is the change in polarization due to an applied field. The effect of displacement of the charge can be found using Eq. **2.1,** where P_o is the spontaneous (initial) polarization, $\chi^{(n)}$ is the nth order susceptibility, and E_n are the applied electric field. When small fields are applied, the spontaneous polarization and the first order susceptibility terms will be dominate and the other terms can be ignored. In stronger fields, the second and third order susceptibilities need to be included. However, the orders higher than third become difficult to discern in realistic situations and can then be disregard [**3**].

$$P_i = P_o + \chi_{ij}^{(1)} E_j + \chi_{ijk}^{(2)} E_j E_k + \chi_{ijkl}^{(3)} E_j E_k E_l + \ldots$$

- Where: P_o is the spontaneous (initial) polarization
  $\chi^{(n)}$ is the nth order susceptibility
  E_n is the applied electric field

(Eq. **2.1**)

The electro-optic (EO) effect is an NLO effect that causes a change in the index of refraction with respect to an applied external electric field. The presence of the electric field disrupts the normal electron motion of the molecules of the substance. This disruption results in a change of the optical properties. Normally, the change in index of refraction is relatively small [**7**]. The index of refraction can be expressed as a function of external electrical field in the form of a Taylor series. This can be seen in Eq. **2.2** where n is the initial index of refraction (where E = 0), r is the linear EO effect coefficient, λ_o is the wavelength in a vacuum, and K is the exponential (or quadric) EO effect coefficient. In most cases, the third order and higher EO coefficients are extremely small in practical fields and therefore ignored.

$$n(E) = n + r \cdot E + \lambda_o K \cdot E^2 + \ldots$$

- Where: n is the initial index of refraction
  r is the linear EO effect coefficient
  λ_o is the wavelength in a vacuum
  K is the exponential EO effect coefficient

(Eq. **2.2**)

The two different coefficients of EO effect that are important are the linear EO effect, r, (known as the Pockels effect) and the quadratic EO effect, K (known as the Kerr effect). The change of n for the Pockels effect is directly related to the applied electric field, while the Kerr effect is related to the square of the applied electric field. Eq. **2.3** and Eq. **2.4** represent the Pockels and Kerr effect, respectively.

$$\Delta n \propto r \cdot E \qquad \text{(Eq. } \mathbf{2.3}\text{)}$$

$$\Delta n \propto (\lambda_o \cdot K)E^2 \qquad \text{(Eq. } \mathbf{2.4}\text{)}$$

Not all materials will have a Pockels effect. If a field E were applied to a material and then reversed direction to $-E$ there would be an equal change in Δn for Equation 2.3. However, there should be some change between E and $-E$ for the Pockels effect to occur (i.e., $r \neq 0$). This means that the structure must have asymmetric properties to demonstrate the Pockels effect. All materials that have centric symmetry and all noncrystalline materials (e.g. polymers and glasses) will not have the Pockels effect. Nevertheless, due to its quadric nature, the Kerr effect is expected in all materials [**7**].

The change in index of refraction can be affected by the direction of applied electric field. When the electric field is applied in the same direction as the incident light beam, this is called longitudinal EO effect. When the electric field is applied in a transverse direction of the incident light beam, this is called the transverse EO effect. For the transverse effect, linearly polarized light will become circularly polarized when it propagates through the material. This happens because both the x- and y-directions of the incident beam will be affected by the electric field [**7**].

Polar Polymeric Material Properties

The use of organic dye chromophores in a polymer system have began to receive more attention due to their potential to generate a large electro-optic effect. The chromophores are typically molecular structures that contain electron donors and acceptors on their ends and create a dipole moment [**8**]. The donor and acceptor electrons

can be aligned by applying an electric field on the chromophore. Separating the donor and acceptor electrons is a conjugated-π bond system. The conjugated-π bond system is an alternating series of single and double covalent bonds in molecular structure. In the system, the p-orbital of all the atoms are aligned in a parallel structure, thus reducing the overall energy of the molecule and increasing the stability. The overall NLO activity can be controlled in the design of the chromophore. This is done by altering certain aspects of the molecular structure (e.g. changing bond length, changing strength of donor and acceptor electrons, etc) to increase the hyperpolarizability of the system [**3**]. Fig. **2.1** shows an example of the organic chromophore *N*-Ethyl-*N*-(2-hydroxyethyl)-4-(4-nitrophenylazo)aniline (commonly known as Disperse Red 1 or DR1).

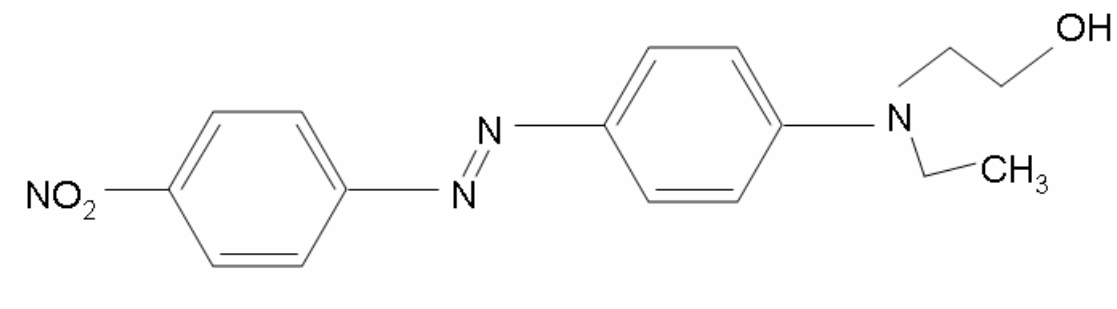

Fig. **2.1**: Illustration of NLO organic chromophore N-Ethyl-N-(2-hydroxyethyl)-4-(4-nitrophenylazo)aniline. This organic chromphore is commonly referred to as Disperse Red 1 or DR-1.

One method to incorporate the chromophore into the polymer is to directly mix it into the polymer matrix during fabrication. This method is called a guest-host system. The advantages of this system are that they are inexpensive to produce, have low dielectric constants and have a large range of operating frequencies. The major disadvantage of this system is a large drop in the glass transition temperature (T_g) due to

the addition of plasticizing effect the smaller chromophore molecules have on the polymer [**3**]. As the percentage of the chromophore present in the system increases the T_g decreases to a point where it is at or below room temperature. At this overloaded point, the NLO activities will have leveled off [**4**].

Another commonly used method is to crosslink the chromophore molecule directly with either the side-chain or main-chain of the polymer via covalent bonding. This can be advantageous due to the fact that it reduces the plasticizing effect by directly linking the chromophore to the polymer. By doing this, the T_g for the system does not decrease making the system more thermally stable. This allows for systems to contain a much larger percentage of chromophore than when compared to the guest-host systems [**9**]. The disadvantages for these systems are that they are more difficult to fabricate and have an elevated cost associated with the chemical needed to properly crosslink the chromophore with the polymer [**5**].

The physical properties of the polymer system can be derived by choosing what polymer and chromophore to use. Many different polymers, including amorphous polycarbonate [**4**] [**2**] and poly(methyl methacrylate) [**9**], and chromophores, including DH-6 and DR1, are used for the polymer-chromophore systems. An important factor is to find a polymer and chromophore that are compatible. This can help compose a system that will maintain a higher T_g [**4**]. Also, selecting a system that operates well at the desired wavelength is important to help reduce optical loss [**2**].

Poly(methyl methacrylate), or PMMA, is a glassy organic polymer that has been recently used for many optical devices. PMMA is used in EO devices and experiments due to its intrinsic nonlinear properties and its ability to act as a host for guest materials

with greater nonlinear properties [**10**]. Also, PMMA has been attractive due to its relative easy fabrication process and inexpensive cost. Fig. **2.2** is a diagram of the PMMA backbone. When using the guest-host setup, the chromophore attaches itself to the polymer backbone in a way that can help enhance the systems NLO activity. An example of this can be seen in Fig. **2.3** which is an example of the chromophore DR-1 attaching itself to a PMMA backbone.

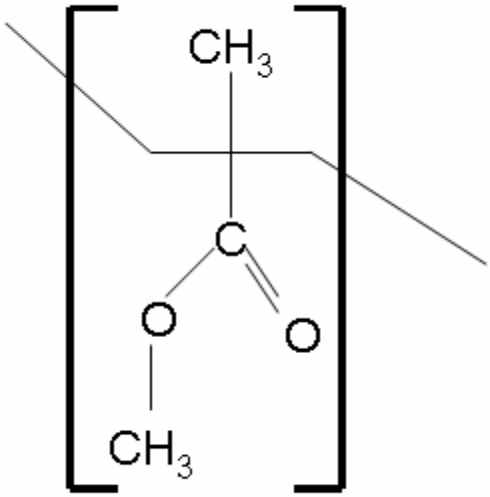

Fig. **2.2**: Basic chemically structure for a chain of poly(methyl methacrlyate) (PMMA).

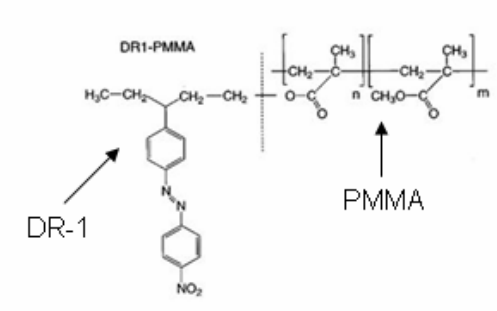

Fig. **2.3**: Illustration of DR-1 chromophore attached to PMMA backbone [**11**].

The introduction of the chromophore to the polymer structure affects the overall nonlinear polarization of the polymer solution on a molecular level. The molecular nonlinear polarization level is described in Eq. **2.5**, where μ_1^0 is the static molecular dipole moment, α_{IJ} is the linear polarizability, β_{IJK} is the first order hyperpolarizability, and γ_{IJKL} is the second order hyperpolarizability [**3**]. The linear polarizability and hyperpolarizability terms refer to an absolute change (either in a negative or positive direction) in the potential of the material. Ideally, maximizing the polarizability and hyperpolarizability values will increase the level of NLO activity in the material. The susceptibility from the overall nonlinear polarization (Equation 2.1) are related to molecular polarizability, $\alpha_{IJ,}$ and hyperpolarizabilities, β_{IJK} and γ_{IJKL}, where α_{IJ} is connected to $\chi^{(1)}$, β_{IJK} to $\chi^{(2)}$, and γ_{IJKL} to $\chi^{(3)}$ [**3**]. These relationships link the molecular polarization directly to overall polarization of the material.

$$p = \mu_1^0 + \alpha_{IJ}E_J + \beta_{IJK}E_JE_K + \gamma_{IJKL}E_JE_KE_L + \ldots$$

- Where: p is the molecular level polarization
  μ_1^0 is the static molecular dipole moment
  α_{IJ} is the linear polarizability
  β_{IJK} is the first order hyperpolarizability
  γ_{IJKL} is the second order hyperpolarizability
  E_n is the applied electric field

(Eq. **2.5**)

The orientation of the dipole moment in the chromophore can be controlled by applying an external electric field to the polymer/chromophore mixture. This can be done by heating the sample up to just below its T_g. By applying the electric field near the T_g, the chromophores can begin to twist in the polymer structure (due to the "liquid-like" state that the system is in), increasing the overall nonlinear polarization of the system [**12**]. After the electric field is applied for a predetermined time, the temperature is

slowly decreased to room temperature. As the temperature is decreased, the motion that was caused by the electric field freezes and becomes permanent. There are various methods for this application, including corona poling [**12**] [**13**], contact poling [**14**], and pulsed poling [**15**].

Chapter 3

Experimental Background Information

Dielectric Properties

Dielectric dispersion is the frequency dependence of dielectric property caused by a change in molecular level polarization with respect to the changing electric field. The relaxation peak is dependent on the frequency of the measurement and will shift with a change in the frequency. The peak can be seen in the graph of the dielectric loss factor (ε") and can be seen in Fig. **3.1**. For most dielectric materials, there are many modes of the relaxation that can be observed, including the ones caused by space charge and dipole polarization. The frequency range for dielectric relaxation can vary from 10^{-5} Hz up to 10^{17} Hz, depending on the relaxation mode. Fig. **3.1** is an example of the frequency response of a dielectric material and the various relaxation mechanisms.

In polymeric materials, two different relaxations can sometimes be observed, above and below the T_g [**16**]. When the temperature is above the T_g, the polymer will start to have "liquid-like" properties (e.g. high viscosity and less rigid). The transition that occurs when the temperature is higher than T_g is referred to as the α relaxation. The α relaxation is linked to the T_g motion of the main chain of the polymer [**8**]. This relaxation can typically be observed easily in most polymers and occurs for most frequencies. The transition that happens below the T_g is referred to as the β relaxation.

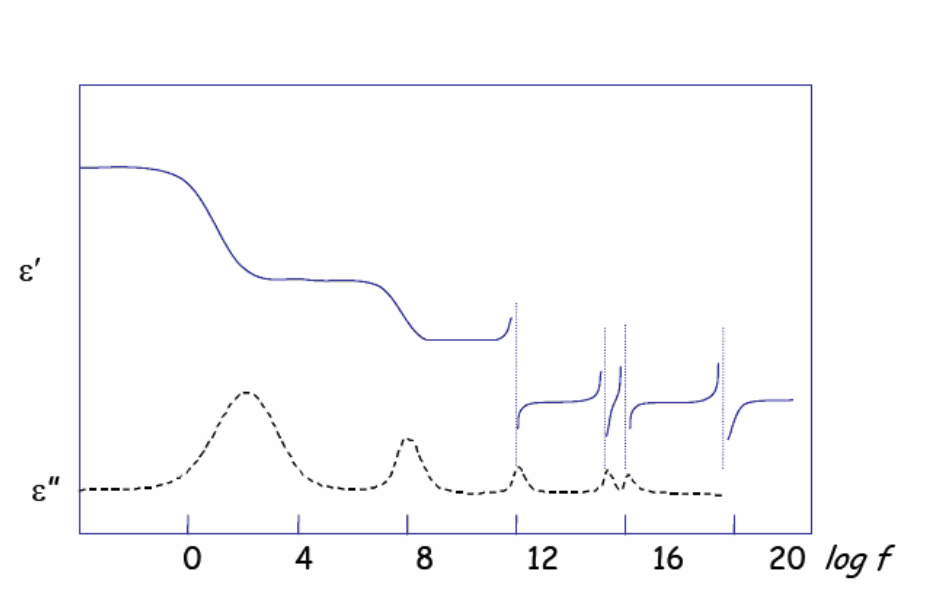

Fig. **3.1**: Example of the frequency response for a dielectric material. The relaxation peaks can be observed in the loss factor (ε").

For polymers, the β relaxation is related to the twisting and aligning of a side chain of the polymer (in the case of PMMA, the relaxation is related to the motion of the -$COOCH_3$ side chain [**8**]). Depending on the T_g of the polymer, the β relaxation can be more difficult to see than the α relaxation. Also, the β relaxation motion will be restricted by doping the polymer with a chromophore (due to lowering of the T_g by the added chromophore). Another way to distinguish the α and β peaks are the α relaxation peaks are narrow and have a sharper peak while the β relaxation are broader and have a less defined peak [**16**].

Another important property linked to dielectric relaxation of materials is the activation energy. The activation energy is the height of the energy barrier required to overcome the relaxation. The activation energy can be found by using the Arrhenius equation. The Arrhenius equation relates the frequency of the relaxation to the

temperature at which the peak occurs and the activation energy. Eq. **3.1** is the Arrhenius equation, where f_o is the frequency of the relaxation, A is a prefactor, E_a is the activation energy, R is the gas constant (8.314472 J/K·mol), and T is the temperature (in Kelvin). The Arrhenius equation can be plotted in the form of a log of the frequency ($log\, f_o$) versus the inverse temperature ($1/T$) using a linear best-fit line. These plots are called Arrhenius plots. The advantage of the Arrhenius plot is that both the activation energy and prefactor can be determined from the graph. The slope of the line will be the activation energy for the relaxation process and the y-intercept will be the prefactor. Eq. **3.1** is used to model the relaxation of the samples in Chapter 4.

$$f_o = A \cdot e^{-\frac{E_a}{R \cdot T}}$$

- Where: f_o is the frequency of the relaxation
  A is a prefactor
  E_a is the activation energy
  R is the gas constant (8.314472 J/K·mol)
  T is the temperature (in Kelvin)

(Eq. **3.1**)

Optical Properties

The static index of refraction for the samples can be physically measured (as opposed to approximating the index of refraction using the relative dielectric constant extrapolated to optical frequency) using ellipsometry. Ellipsometry is a measurement technique that uses elliptically polarized light to characterize materials. The principle behind ellipsometry is that the light source (usually a laser) strikes the material at a predetermined angle. The light passes through the material and then is reflected into a photo detector that collects the optical intensity. Using modeling equations, the index of

refraction and thickness of the material can be measured. The thickness measurements are very precise with ellipsometry and typically can measure at the Angstrom range. The precision of the ellipsometry measurement makes it popular with thin film characterizations.

One technique for making optical measurements is the Michelson interferometer method. A Michelson interferometer is a setup that splits an incident beam (using a 50/50 non-polarizing beam splitter) into two beams, the reference arm and the sample arm, with equal intensity. A basic diagram of the Michelson interferometer set up can be seen in Fig. **3.2**. A Michelson interferometer uses the principle of superposition to create a constructive or destructive interference pattern. The interference pattern is dependent on the difference of the two optical beam paths, which can be modeled by the overall phase. The pattern can be broken down into terms of the maximum (constructive interference) and minimum (destructive interference) light intensities of the two arms of the interferometer. The important points are the so-called $\lambda/4$ wave points. These are the points in the measurement where the interference light intensity is maximized. The overall change of path will then be related linearly to change in the interference intensity. Using this information, the change in the index of refraction can then be measured by obtaining the peak-to-peak voltage of the interference pattern and the ac voltage that is output to the sample.

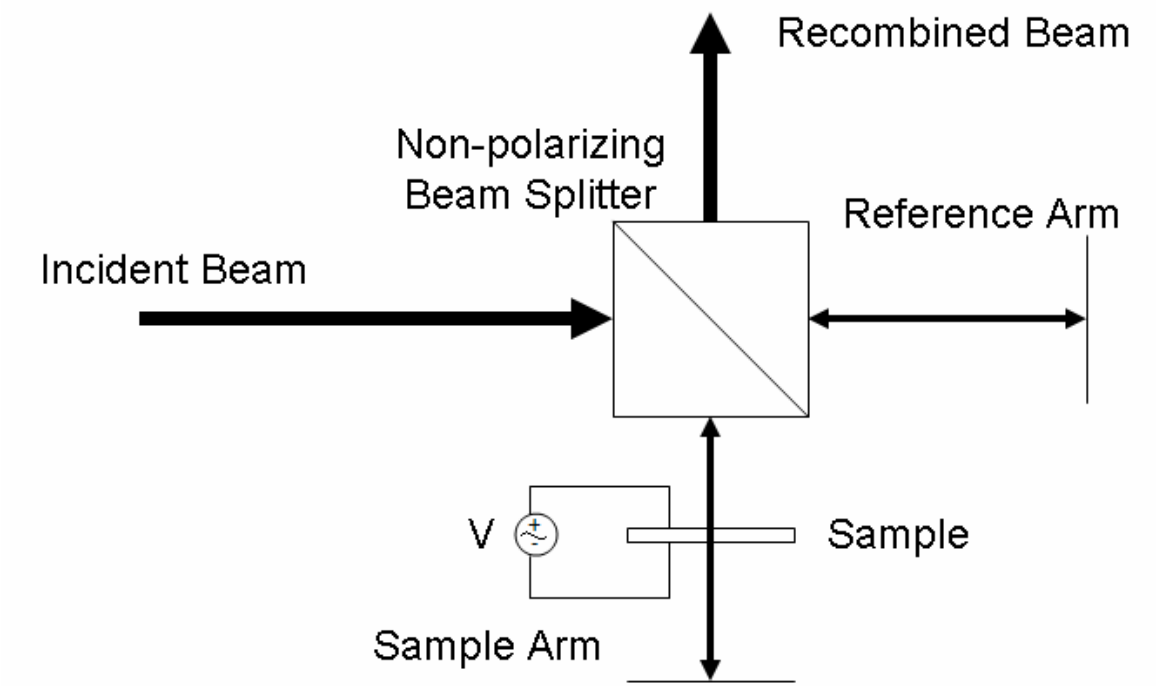

Fig. **3.2**: Michelson interferometer setup.

The Kerr EO effect can be found experimentally, using the aforementioned technique, by calculating the phase difference of the light source as it passes through the sample. The phase change can be found using Eq. **3.2**, where φ is the phase difference, Δn is the change in the index of refraction, l is the length of affected optical path, λ is the wavelength, E is the applied electric field, and K is the Kerr coefficient [**17**].

$$\varphi = \frac{2\pi}{\lambda} \cdot \Delta n \cdot l = 2\pi \cdot K \cdot l \cdot E^2 \qquad \text{(Eq. 3.2)}$$

- Where: φ is the phase difference
  Δn is the change in the index of refraction
  l is the length of affected optical path
  λ is the wavelength
  E is the applied electric field
  K is the Kerr coefficient

Chapter 4

Experimental Measurements and Results

Material Preparation and Fabrication

A guest-host polymer system was used for the system. The polymer, PMMA, used for the polymer part of the system was purchased from Scientific Polymer Products (MW = 540,000 g/mol) and the chromophore, DR1, used for the chromophore part of the system from Sigma Aldrich. Glass slides with approximately a 150-300 Å transparent layer of indium tin oxide [In_2O_3/SnO_2] (ITO) and a surface resistivity of 70-100 Ω/sq (also purchased from Sigma Aldrich) were used for the substrates. The ITO layer acted as a base electrode for the parallel-plate capacitor model used for the dielectric measurements. The glass slides were chosen for the substrate in this experiment so the optical measurements could be made with a modified Michelson interferometer setup.

The PMMA was stirred and dissolved in the cyclopentanone for 24 hours on a heated stirring plate in a fume hood. After the PMMA was completely dissolved in the solvent, the DR1 was then added to the PMMA/cyclopentanone solution and mixed for 24 hours. As previously mentioned, when the percentage (by weight) of DR1 is 15% or higher, the solution becomes heterogeneous, or multiphase [**8**]. A heterogeneous solution would be more difficult in spin coating due to that the DR-1 does not fully dissolve and forms precipitates. Also, the mixture would not generate as reliable data as a homogeneous mixture one due to the distribution in dielectric permittivity and loss. Due

to these facts, three different solutions were made for this experiment: 0% DR1 (100% pure PMMA), 5% DR1, and 10% DR1. In addition, the overall ratio of the PMMA/DR1 mixture to solvent was important to determine. This ratio determined the overall viscosity of the solution. If the viscosity was too low then the solution would not properly spin on, leaving exposed areas of the substrate. If the viscosity was too high, the solution would not dissolve suitably and leave "streaks" in the polymer layer. Furthermore, if the solution is too thick, it cannot fully spin onto the substrate and will gather at the edges. By testing various PMMA/DR1-to-solvent ratios it was determined that a 10% of the total weight of the solution should be PMMA/DR1 for the best quality and uniform polymer layer.

When the solution was completely dissolved, the ITO-coated glass substrates were cleaned with acetone and blown clean with compressed air. Initially, the polymer was directly applied to the substrate (via spin-coating). This method caused the polymer film to contain air bubbles and other visible impurities. An example of this problem can be seen in Fig. **4.1**. These problems were solved by filtering the solution through a 0.45 μm PTFE filter before spinning the solution onto the glass substrates. One of the major problems with the spin coating method was the solution collecting on the edges of the sample, increasing the thickness of those areas. Possible causes of this were the spinning speed being too slow or the total spinning time was too short. With this occurring, any data collected near the edges would be considerably different than data collected towards the center. An example of this can be seen in Fig. **4.2**. The speed and spinning time of the sample were varied to find a combination that produced the most uniform sample,

both in thickness consistence and visible inspection. 600 RPM for 2 minutes were the spin speed and time chosen for this experiment that produced the most consistent samples. Most of the solvent was evaporated when it was spun onto the glass substrate, leaving a thin polymer layer on top of glass substrate. After spin coating was finished, the samples were set aside to air dry at room temperature. The different trial-and-error steps taken to find the fabrication parameters (10% dry weight for the PMMA/DR-1 for the polymer solution and 2 minutes at 600 RPM for the spin coating) can be found in Appendix A.

Fig. **4.1**: Picture of an air bubble that was formed during the spin coating process.

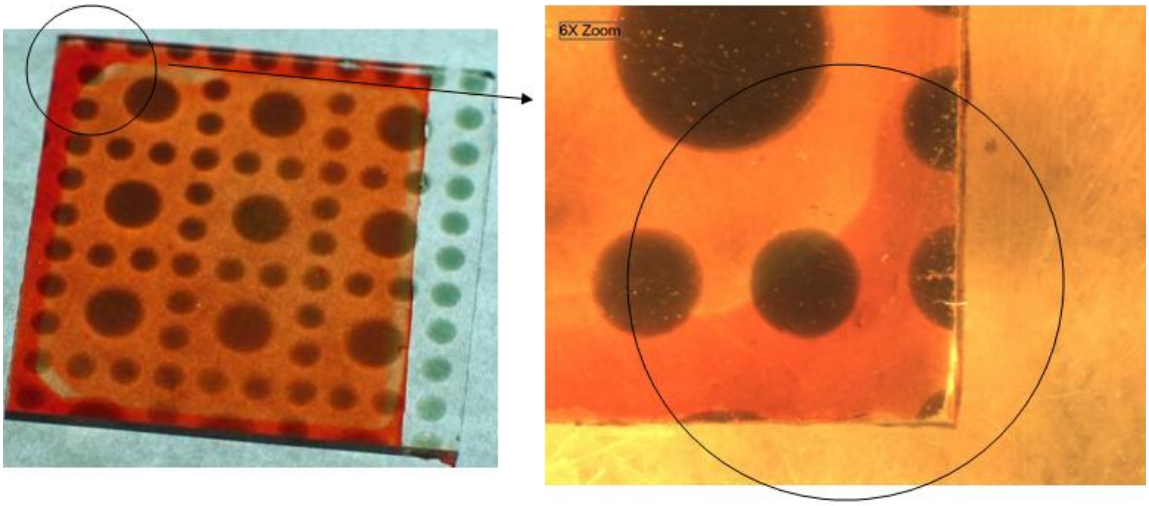

Fig. **4.2**: An example of the polymer film collecting at the edges of the substrate. On the left is the full picture of a sample. The right picture is a magnified view of the upper left cornor of the sample. The circled portion of the left picture is the area where the polymer collected during the spinning process.

Once the polymer solution was completely dried one of the edges of the sample was removed so the base ITO electrode could be exposed. This allowed for the thickness to be measured using a Tencor 500 profilometer. The samples were measured multiple times to check for uniformity of the polymer layer. Initially, the thickness measured on the first polymer solutions had varying thickness and noticeable deformities. After filtering the samples to remove imperfections, the samples were much more uniform and had more of a consistence quality than before. The thicknesses for the measured final samples were between the range of 0.8 μm (thinnest sample) to 1.75 μm (thickest sample) with the relatively small error (+/- 100 nm per sample). In addition, exposing the base ITO electrode permits for samples to be measured on the thin film stage.

Originally, a gold electrode was sputtered on top of the polymer layer to create the parallel-plate capacitor structure. The electrodes were sputtered using a Bal-Tec SCD

050 Sputter Coater and mask with two circular patterns of different sizes (1.5 mm and 3.25 mm diameters). At first, the electrodes were sputtered on using normal sputtering settings (25 mA current for 45 seconds) and this caused the electrodes to puncture the polymer film and shorting the capacitor structure. This was remedied by reducing the current and increasing the time of the sputter. The current was reduced from 25 mA to 5 mA and the time was increased from 45 seconds to 225 seconds. The smaller circles were used for the dielectric and optical measurements due to "pinholes" that were in the polymer structure. The pinholes are microscopic imperfections in the polymer that occurred during the spin-coating process. Fig. **4.3** shows an example of the pinholes spread throughout a unelectroded sample. The smaller electrode size helps decrease the number of electrodes that are shorted. The next problem encountered was that the smaller circular top electrodes (diameter of 1.5 mm) were not large enough for a quality optical measurement to be taken. With the improvement of the polymer film quality, the number of pinholes was reduced and a mask with larger circle patterns (5 mm diameter circles). Finally, the metal used for top electrode was replaced with platinum. A platinum electrode would reduce the amount of reflection in the optical measurement when compared to gold, thus improving the quality of the measurement. Fig. **4.4** shows a diagram of the cross-section of the sample.

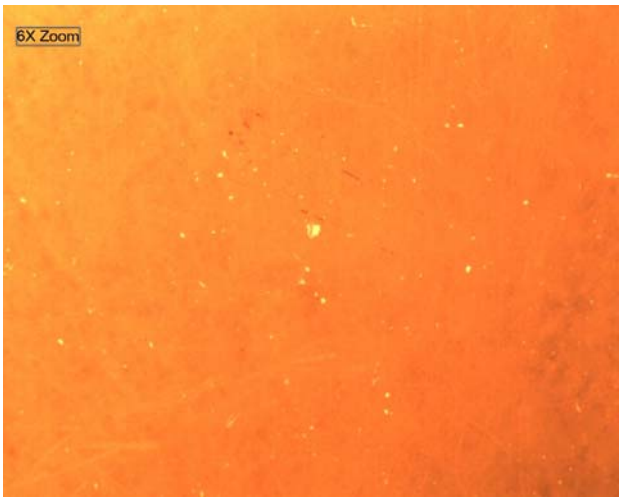

Fig. **4.3**: 6X view of an earlier sample prior to placing top electrodes on via sputtering, showing pinholes throughout polymer layer.

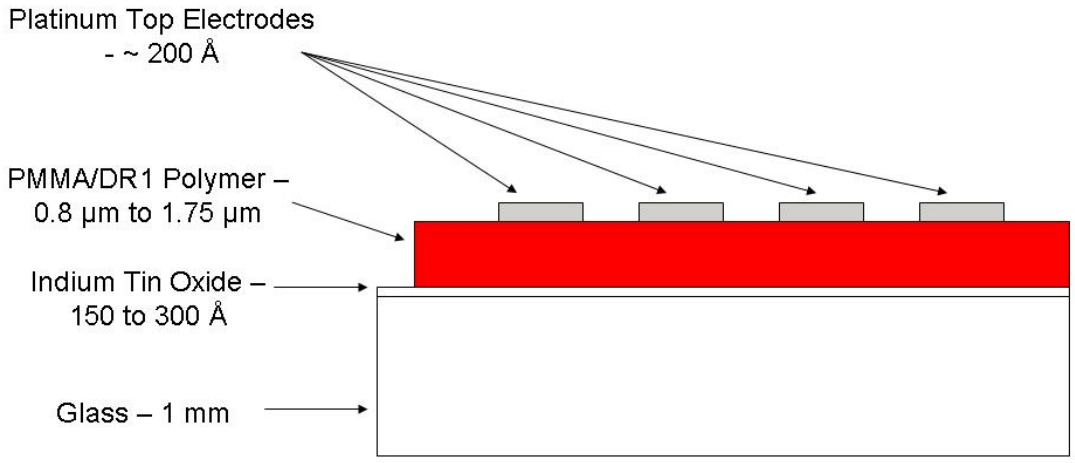

Fig. **4.4**: A diagram of cross section of sample with layer thicknesses (not to scale)

Dielectric Measurements

Frequency Dependence

After the platinum electrodes were sputtered onto the polymer, the frequency dependent dielectric properties were measured using Hewlett-Packard Model 4284A precision LCR meter. The HP 4284A LCR meter was used to measure the capacitance and loss tangent, tan δ. The samples were measured using a thin film probe station by placing one probe on the base electrode layer (the ITO layer) and the other probe on one of the platinum top electrodes (located on top of the polymer layer). The capacitance and loss tangent were recorded at 22 different frequencies ranging from 100 Hz to 100 kHz at room temperature (25 °C). The dielectric constant, ε_r, was then calculated by using considering the sample to be a parallel-plate capacitor (Eq. **4.1**) where C is the capacitance in farads, t is the thickness of polymer in meters, ε_o is the permittivity of free space (8.85×10^{-12} F/m), and A is the area of the electrode in meters squared. The loss factor, ε", was then calculated using Eq. **4.2**. The graphs for the relative dielectric constant and loss factor can be seen in Fig. **4.5** and Fig. **4.6**, respectively. Fig. **4.5** shows a consistent increase in the relative dielectric constant with the increased concentration of DR-1. Fig. **4.6** suggests that an optimal concentration level may be located between 5% and 10% DR-1. This is indicated by the slight decrease in the loss factor from the 10% DR-1 sample compared to the 5% DR-1 sample.

$$\varepsilon_r = \frac{C \cdot t}{\varepsilon_o \cdot A}$$

- Where: ε_r is the relative dielectric constant
  C is the capacitance
  t is the thickness of the sample
  ε_o is the permittivity of free space (8.85 x 10^{-12} F/m)
  A is the area of the top electrode

(Eq. **4.1**)

$$\varepsilon'' = \varepsilon_r \cdot \tan\delta$$

- Where: ε'' is the loss factor
  ε_r is the relative dielectric constant
  $tan\ \delta$ is the loss tangent

(Eq. **4.2**)

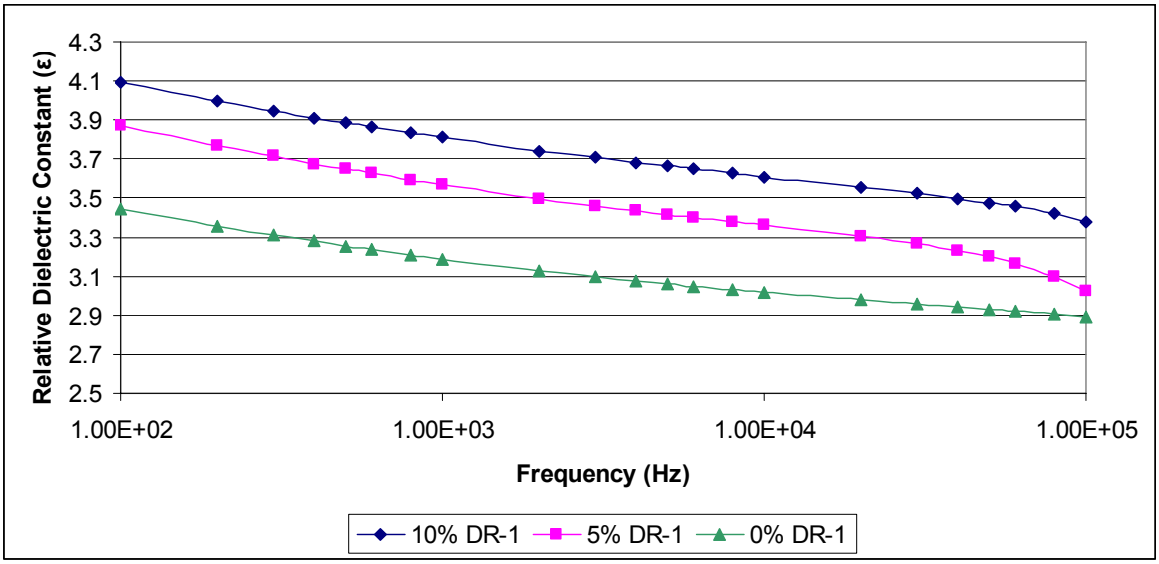

Fig. **4.5**: Frequency dependence measurement of relative dielectric constant. The measurement was done for all three concentrations (0% DR-1, 5% DR-1, and 10% DR-1) for 22 different frequencies from 100 Hz to 100 kHz.

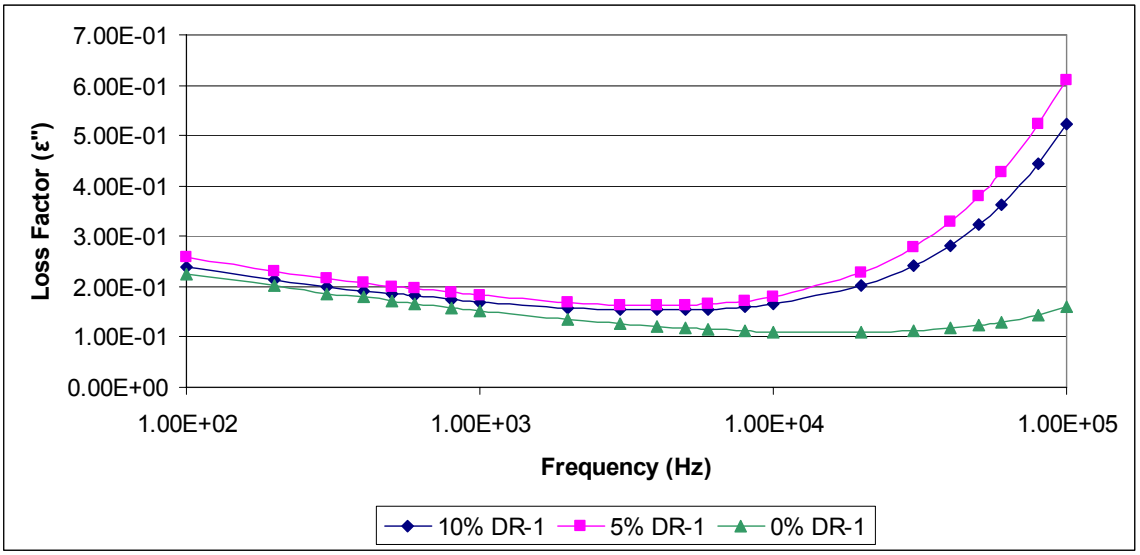

Fig. **4.6**: Frequency dependence measurement of dielectric loss factor. The measurement was done for all three concentrations (0% DR-1, 5% DR-1, and 10% DR-1) for 22 different frequencies from 100 Hz to 100 kHz.

The index of refraction, n, can be related to the materials dielectric constant. For the case of dielectric measurements, the relation can be described as Eq. **4.3**, with μ_r being the relative permeability. The relative dielectric constant can be written as an addition of the static dielectric constant (ε_r) and optical dielectric constant (ε_∞). At optical frequencies, the relative permeability and static dielectric constant are typically equal to 1 for most materials. This leaves the index of refraction to approximately equal the square root of the relative dielectric constant, which is seen in Eq. **4.4**. Using the estimation of Eq. **4.4** and the values found from Eq. **4.1**, the index of refraction can be calculated. A graph of these values can be found in Fig. **4.7**. The relative dielectric constant, loss factor, and estimated index of refraction measurements for all the samples at 1 kHz can be found in Table **4.1**.

$$n = \sqrt{(\varepsilon_r \cdot \mu_r)}$$

- Where: n is the index of refraction
  ε_r is the relative dielectric constant
  μ_r is the relative permeability

(Eq. **4.3**)

$$n \approx \sqrt{(\varepsilon_r - 1)}$$

- where: n is the index of refraction
  ε_r is the relative dielectric constant

(Eq. **4.4**)

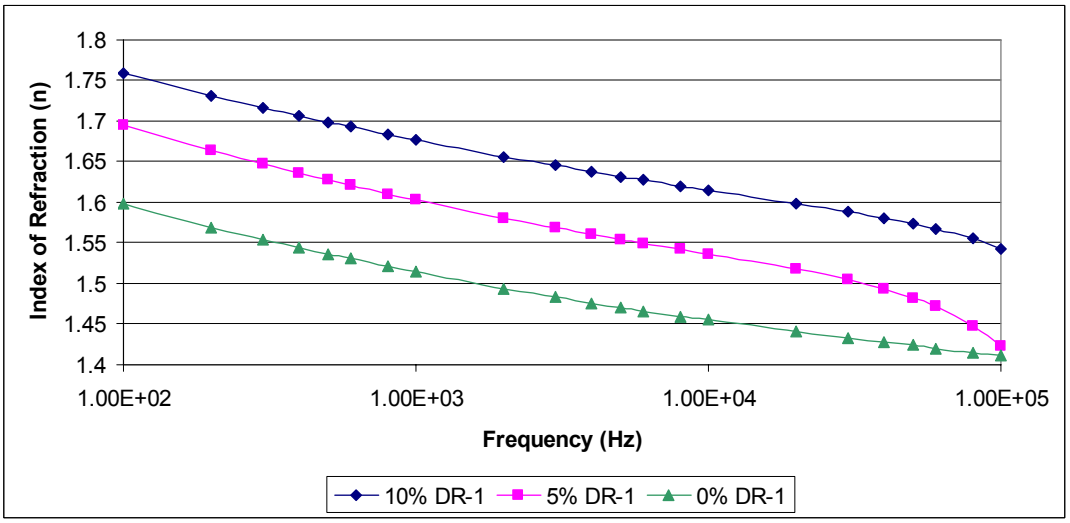

Fig. **4.7**: Approximation of index of refraction using the calculated relative dielectric constant. The estimated index value is for at optical frequencies. The measurement was done for all three concentrations (0% DR-1, 5% DR-1, and 10% DR-1) for 22 different frequencies from 100 Hz to 100 kHz.

Table **4.1**: Frequency dependence measurements for all samples at 1 kHz. The relative dielectric constant consistently increases with the addition of more DR-1. The decrease in loss factor from 5% DR-1 to 10% DR-1 indicates that an optimal DR-1 concentration may be located somewhere between those values.

Sample	Relative Dielectric Constant (ε_r)	Dielectric Loss Factor (tan δ)	Estimated Index of Refraction
0% DR-1	3.188	4.41%	1.521
5% DR-1	3.569	5.01%	1.602
10% DR-1	3.833	4.45%	1.673

Temperature Dependence

The dielectric temperature dependency of the samples were measured by measuring the relative dielectric constant and loss factor while increasing the temperature from room temperature (~25 °C) to 150 °C in increments of 2 °C per minute. The samples were heated using a thin film heating stage and the dielectric measurements were done using the same setup and method as mentioned in the Frequency Dependent Measurement section.

As discussed earlier, the glass transition temperature, T_g, is the temperature when the polymer material starts to act more "liquid-like". The T_g value for PMMA and PMMA/DR-1 mixtures are well documented using the DTA method. For Lei et al [**8**], PMMA (0% DR-1), the T_g is reported at approximately 100 °C, for a 5% PMMA/DR-1 mixture, the T_g is reported at approximately 90 °C, and for a 10% PMMA/DR-1 mixture, the T_g is reported at approximately 80 °C. An issue that initially occurred in this

dielectric measurement was the polymer became too soft at higher temperature (above 120 °C) and the probe began to puncture the polymer. This was remedied by placing a small piece of aluminum foil on the top electrode to help create a better contact point. The relative dielectric constant and loss factor results can be seen in Fig. **4.8**, (0% DR-1), Fig. **4.9** (5% DR-1), and Fig. **4.10** (10% DR-1).

The α-relaxation peak can prominently be seen in Fig. **4.8**, Fig. **4.9**, and Fig. **4.10** while the β-relaxation peak can be seen at the lower frequencies for the 5% and 10% DR-1 films. An example of both the α- and β-relaxation can be seen in Fig. **4.11** where the β-relaxation occurs at the lower temperature while the α-relaxation occurs at the higher temperature. For the 0% DR-1 sample (pure PMMA), the α and β peaks are overlapped at lower frequencies and harder to discern. This can be seen in Fig. **4.8** for the 100 Hz data. Bergman et al [**18**] discusses this phenomenon in greater detail. Due to this issue, the α-peak of the 0% DR-1 sample was ignored. The peaks are separated and more distinct for the 5% and 10% samples due to the lower T_g caused by the plasticizing effect the DR-1 chromophore has on the PMMA. Using the Arrhenius equation (Eq. **3.1**), the α- and β-loss peaks were graphed by plotting the natural log of the frequency peaks versus the inverse of the temperature at which they occur (Fig. **4.12**). The activation energy is equal to the slope of linear line connecting the points on the graph.

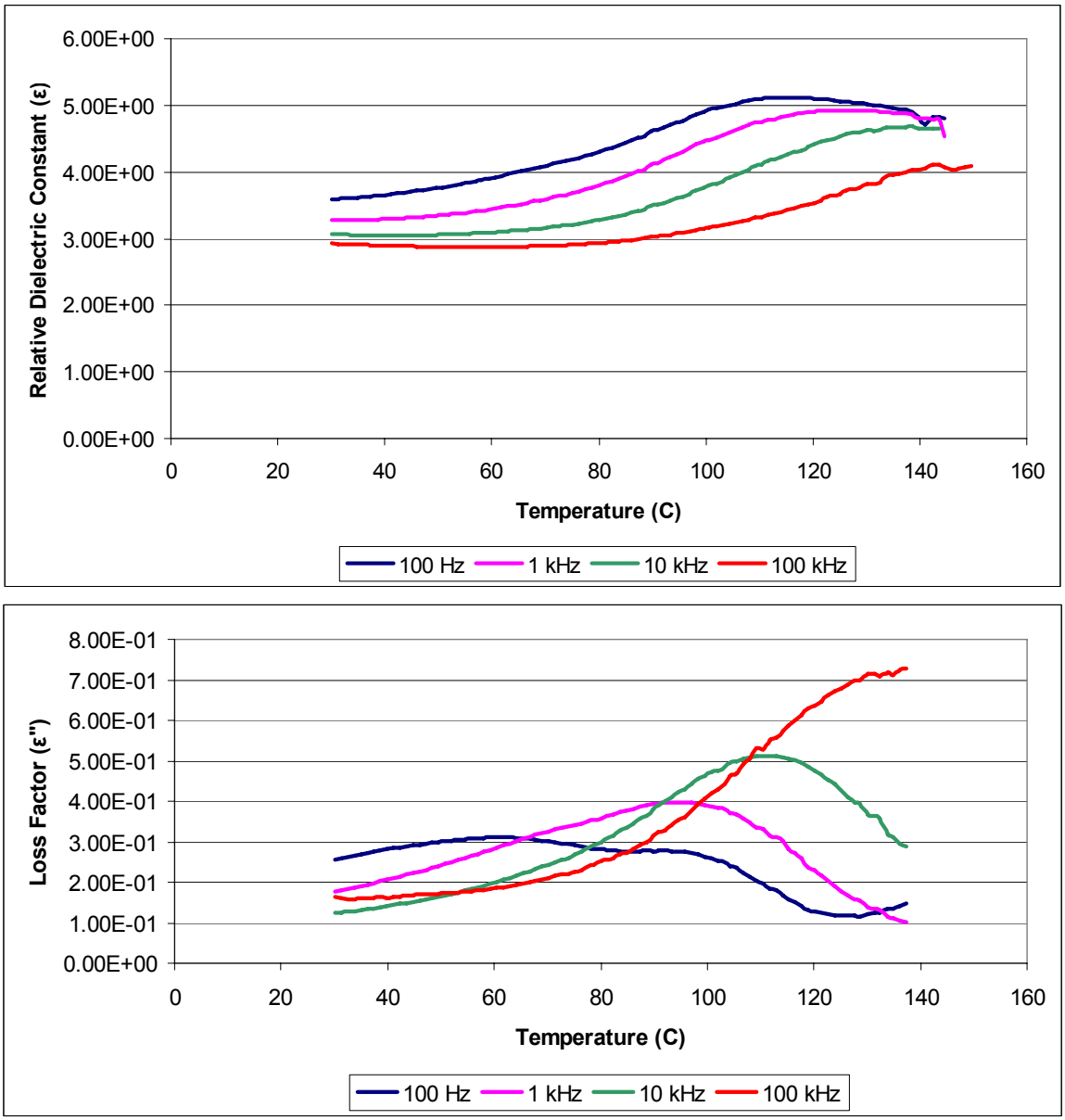

Fig. **4.8**: Temperature dependence dielectric measurement for sample with 0% DR-1. (Top) Relative dielectric constant, (Bottom) Loss factor. The temperature started at 30 °C and was increased to 150 °C. The relaxation can be observed in the loss factor graph.

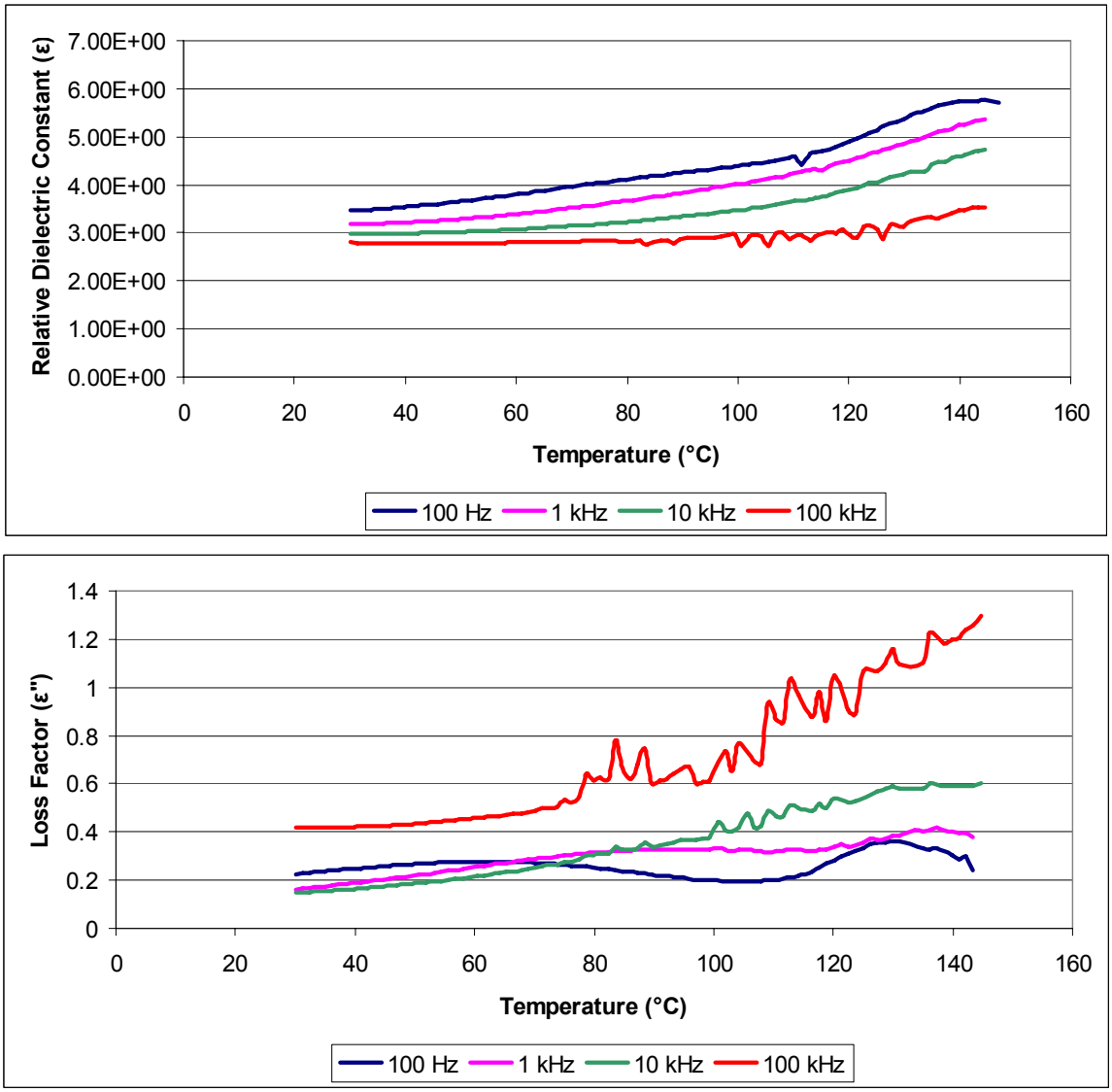

Fig. **4.9**: Temperature dependence dielectric measurement for sample with 5% DR-1. (Top) Relative dielectric constant, (Bottom) Loss factor. The temperature started at 30 °C and was increased to 150 °C. The relaxation can be observed in the loss factor graph.

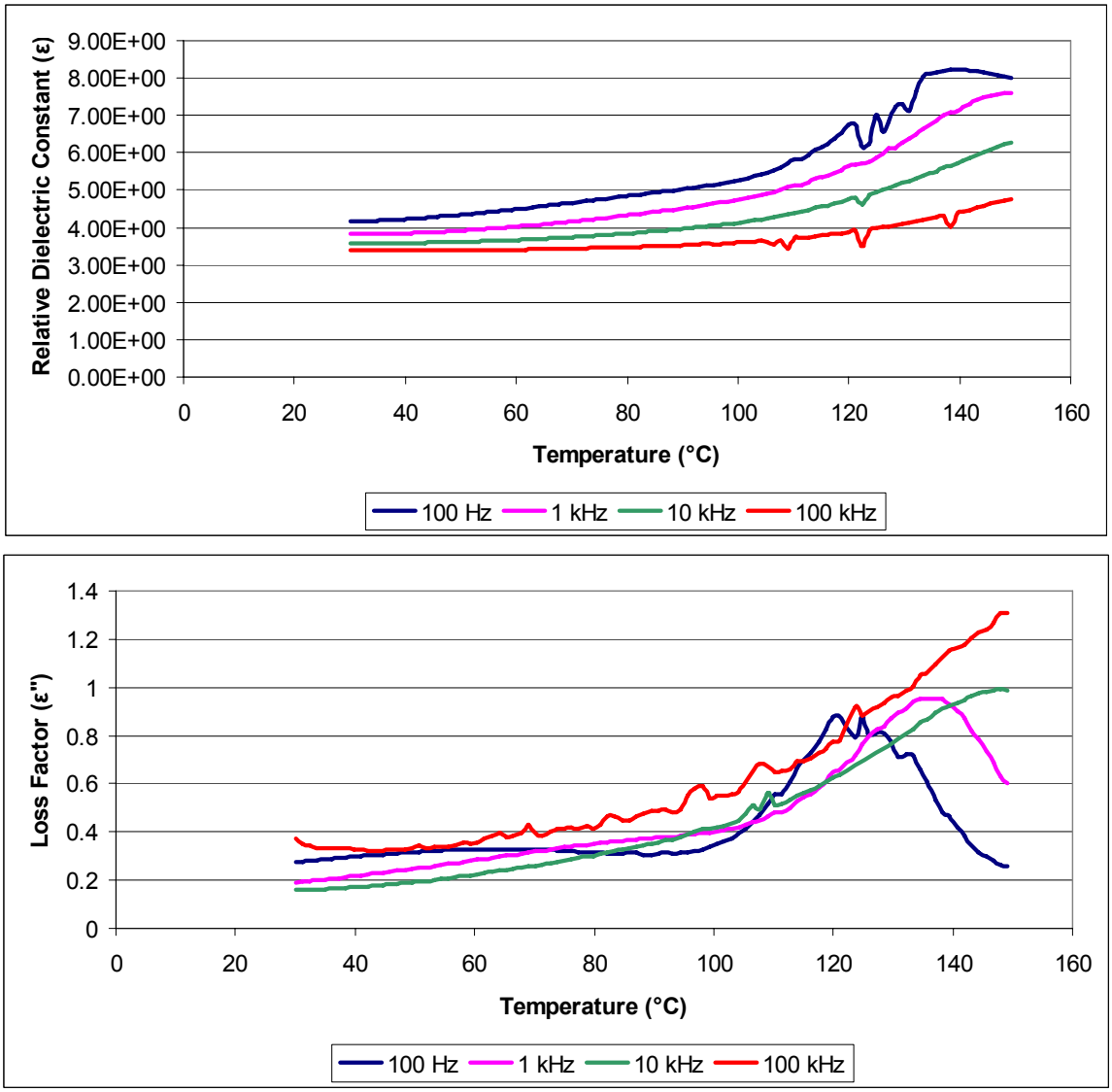

Fig. **4.10**: Temperature dependence dielectric measurement for sample with 10% DR-1. (Top) Relative dielectric constant, (Bottom) Loss factor. The temperature started at 30 °C and was increased to 150 °C. The relaxation can be observed in the loss factor graph.

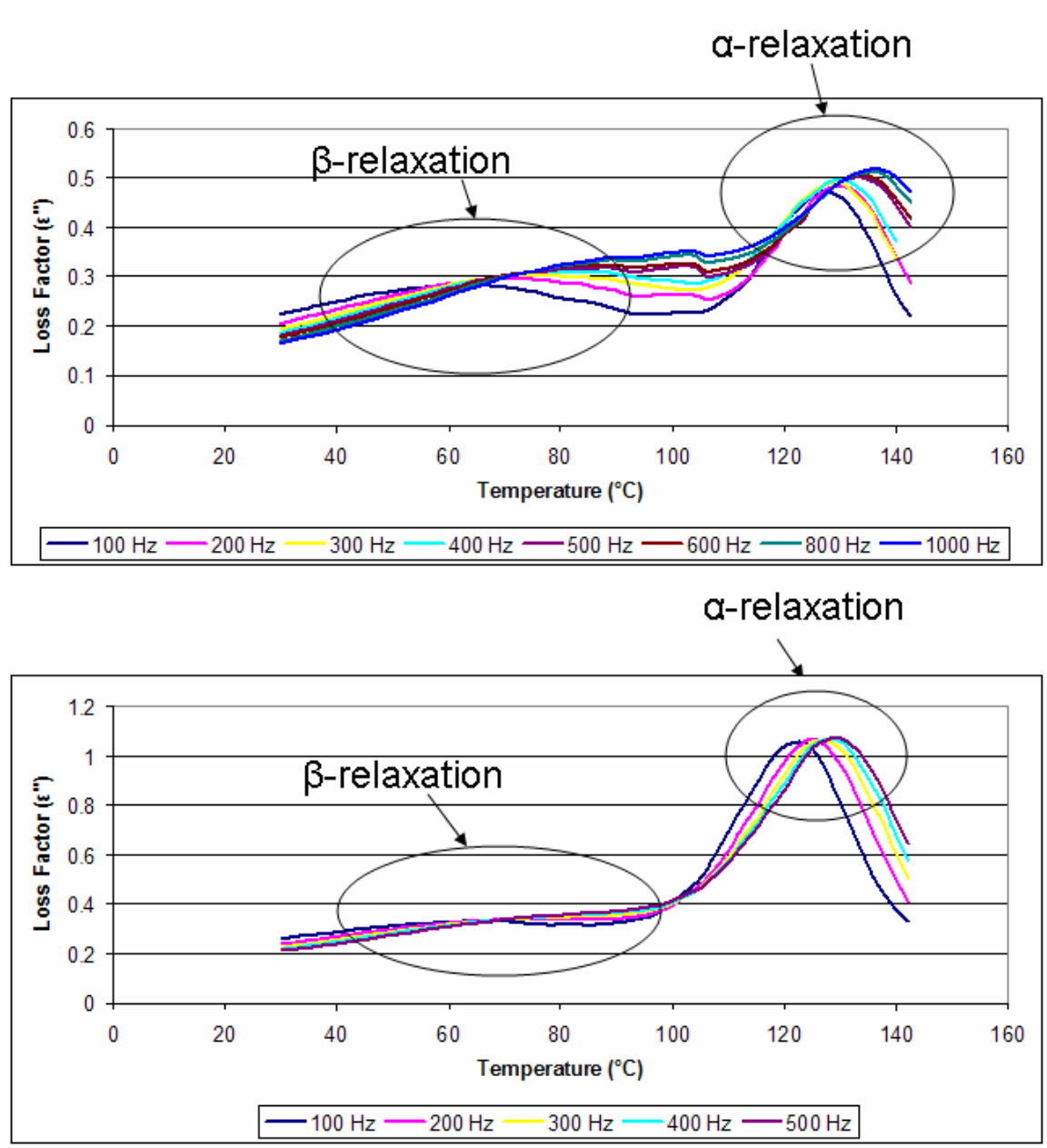

Fig. **4.11**: α- and β-relaxation for 5% DR-1 (top) and 10% (bottom) samples.

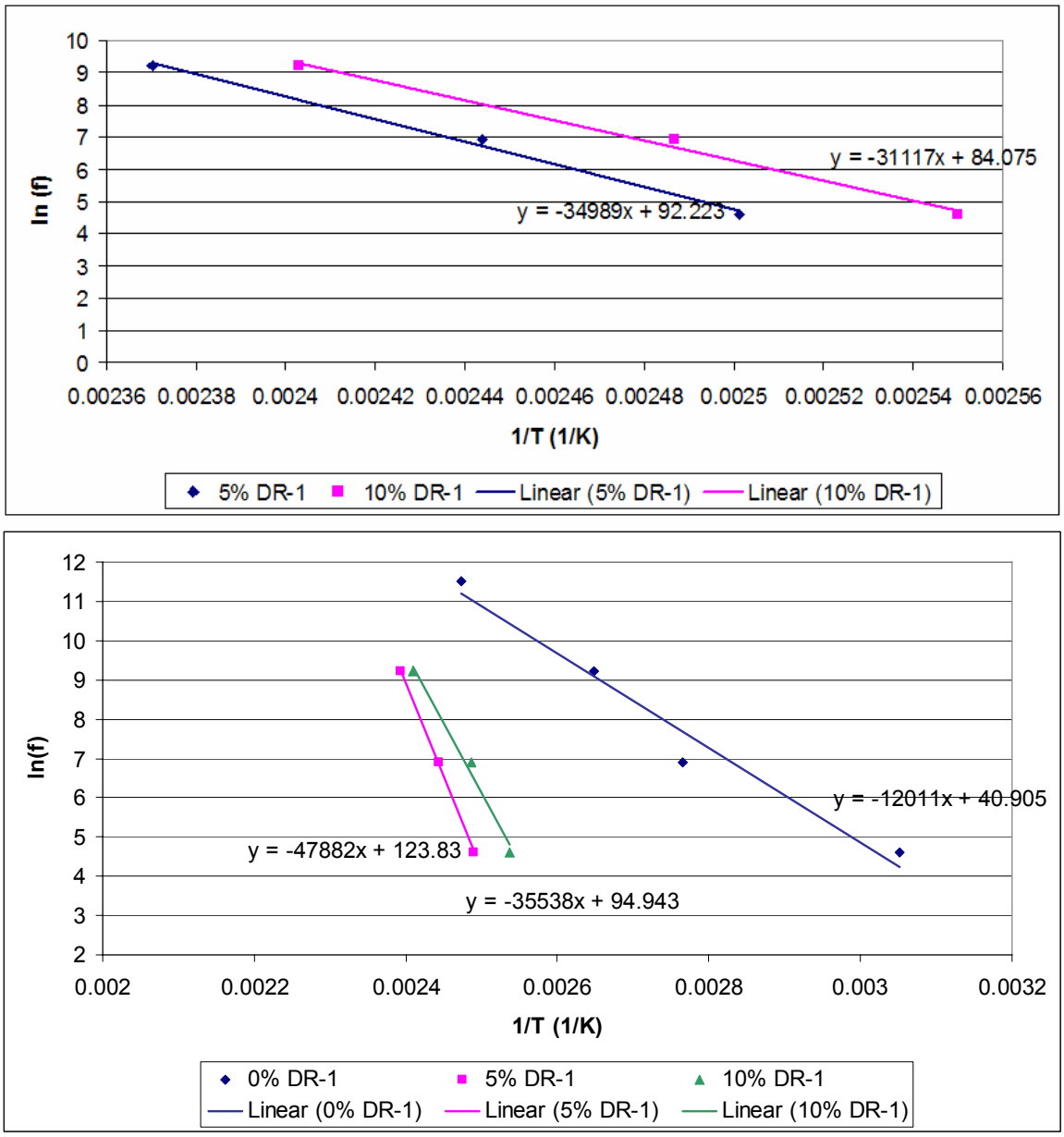

Fig. **4.12**: Arrhenius plot for α-relaxation peaks (top) and β-relaxation (bottom).

Using the slope-intercept equations from the Arrhenius plot, the activation energies were calculated. The various activation energies obtained are summarized in Table **4.2**. Lei et al [**8**] reported the α activation energy for the 5% and 10% DR-1 samples to be 69 kcal/mol and 58 kcal/mol, respectively. The β activation energy for 0%,

5%, and 10% DR-1 sample were reported at 21 kcal/mol, 11 kcal/mol, and 10 kcal/mol, respectively. The reduction in the activation energy for both the α and β relaxation mechanism shows that the introduction of the DR-1 chromophore effects both the motion of the main chain (which changes the T_g of the polymer) and the motion of the side chain.

Table **4.2**: Activation energy for α and β relaxation process. The activation energy decreases as the amount of chromophore is increased, similar to the reported values. Reported values from Lei et al [**8**].

Percent DR-1	Measured α Activation Energy (kcal/mol)	Reported α Activation Energy (kcal/mol)	Measured β Activation Energy (kcal/mol)	Reported β Activation Energy (kcal/mol)
0	-	-	23.87	21
5	69.52	69	17.38	11
10	61.83	58	14.67	10

DC Field Bias Measurements

An applied electric field was applied to the sample in an attempt to align the dipole moments of the DR-1 chromophore. Due to the relatively small thickness (~1 μm) of the samples and thus low voltage required, a dc bias voltage was applied to the samples using the dc bias output of the LCR meter. The 40 V output from the LCR was applied to the sample at room temperature and the temperature was slowly increased (~ 2 °C/min) up to 70 °C, slightly below the known T_g. The voltage was held there for 30 minutes and decreased back to room temperature. The capacitance and loss factor were measured after the sample had completely cooled down to room temperature, with the

anticipation that a noticeable change would be caused by the motion of the chromophore. However, no significant change was noticed between the measurements before and after the applied voltage for most samples. The samples began to show breakdown as the capacitance and loss values started to short for thinner samples (thickness less than 1 μm).

A polarization versus electric field (P-E) measurements was then done to examine and see if the applied electric field had caused any nonlinear behavior within the polymer. An electric field (in the form of a sine wave) was applied to the samples and the polarization charge was then measured. This was done both at room temperature and at 70 °C for the 5% and 10% DR-1 samples. The P-E measurements were taken at lower frequencies. The 1 kHz measurements can be seen in Fig. **4.13**. The figure shows that there was no significant nonlinear activity created by applying the electric field at room temperature and at a higher temperature. Also, the biased dielectric constant can be related to the P-E measurement. This relationship can be seen in Eq. **4.5**, where P is the polarization, ε_o is the permittivity of free space, and E is the applied electric field. The biased dielectric constant was found by measuring the slope of the P-E graph (Fig. **4.13**). Fig. **4.14** illustrates a graph of the biased dielectric constant plotted versus the electric field. The small change in the biased dielectric constant also indicates that no considerable dielectric activity was present.

$$\varepsilon_r^{bias} = \frac{P}{\varepsilon_o E} \qquad \text{(Eq. 4.5)}$$

- Where: ε_r^{bias} is the bias dielectric constant
  P is the polarization charge
  ε_o is the permittivity of free space (8.85×10^{-12} F/m)
  E is the applied electric field

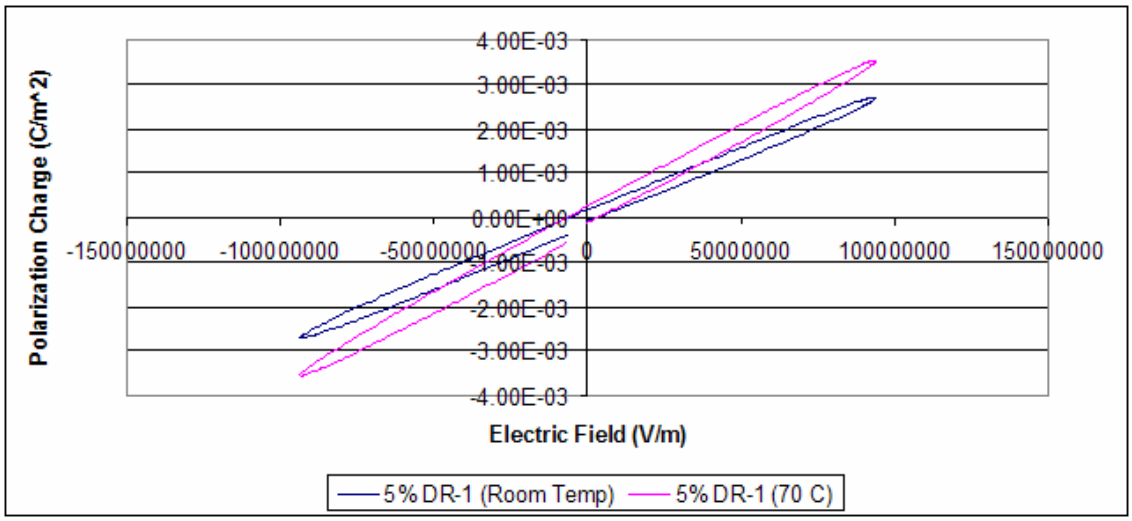

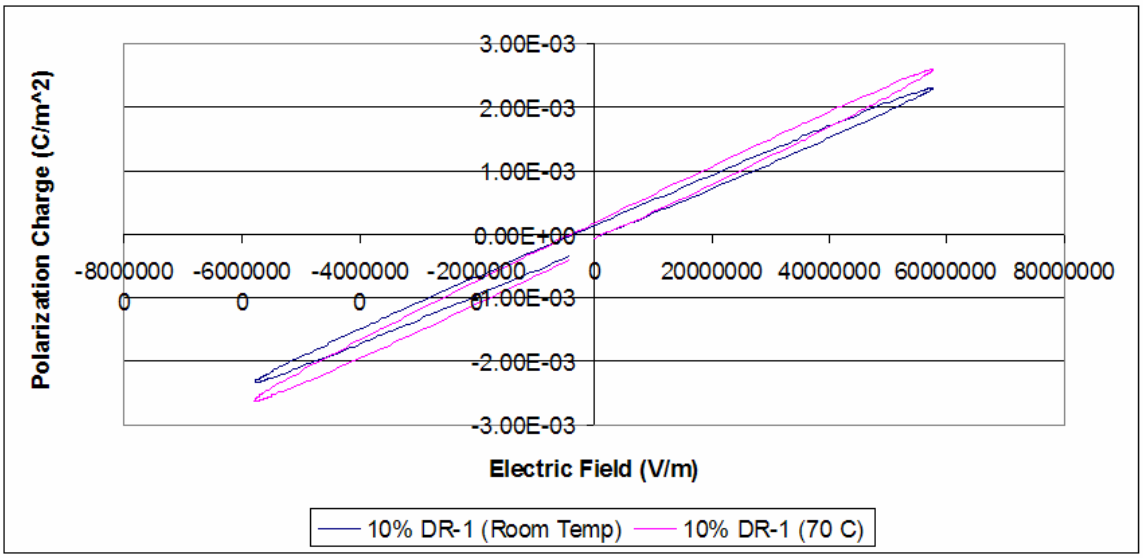

Fig. **4.13**: P-E graph for 5% DR-1 sample (top) and 10% DR-1 sample (bottom). The field was applied as a sine wave. A slight nonlinearity can be seen forming at the higher electric field.

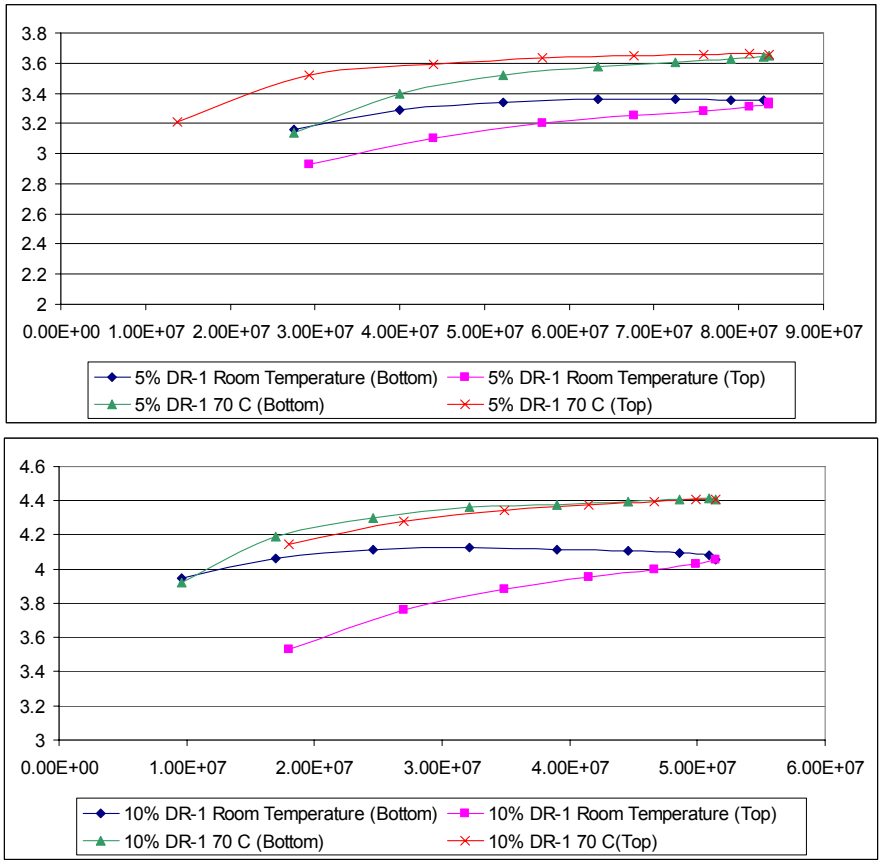

Fig. **4.14**: Biased dielectric constant versus electric field for 5% DR-1 (top) and 10% DR-1 (bottom). The minimal change in the biased dielectric constant indicates that there is only minor nonlinear activity in the sample.

The lack of significant nonlinear activity, along with the thinner samples breaking down, show that generating an applied electric field to properly induce motion that freezes into place with the current polymer structure may not be possible. A slight nonlinearity can be seen at the higher applied electric field (Fig. **4.13**). This may indicate that the dipole moments of the chromophore began to realign and create nonlinear activity. However, the area was not significant enough to generate any considerable nonlinear activity.

Optical Measurements

Normalized Index of Refraction

The index of refraction for the 5% and 10% PMMA/DR-1 samples were measured multiple times using an ellipsometer. A Gaertner L116D Variable Angle Microfocus Ellipsometer was used for this measurement. Using a computer modeling program and the measured thickness, the index was calculated. The measurement was repeated more four times on different areas of sample. The results for these measurements can be found in Table **4.3**. The average index of refraction for the 5% DR-1 samples was 1.610, while the average index of refraction for the 10% DR-1 samples was 1.621. The average index for PMMA is reported at 1.50. The reported index of refraction for a sample containing 7.5% DR-1 was 1.53 [**19**]. These values can be seen compared to the values extracted from the dielectric measurement in Table **4.4**.

Table **4.3**: Normalized index of refraction for 5% DR-1 and 10% DR-1 samples.

Percentage DR-1	Point 1	Point 2	Point 3	Point 4	Point 5
5 % DR-1	1.4684	1.712	1.4965	1.5795	1.6632
5 % DR-1	1.6104	1.7112	1.6059	1.5802	1.6628
10 % DR-1	1.563	1.5219	1.5107	1.5463	1.5221
10 % DR-1	1.7091	1.7119	1.7094	1.7135	1.7077

Table **4.4**: Comparison of estimated index of refraction (from dielectric measurement) to the optically measured index of refraction (from ellipsometry). The values for the 0% DR-1 and 5% DR-1 samples are similar, while the estimated index for 10% DR-1 sample is larger. This could be due to impurities in the film or inconsistence in thickness of the film.

Sample	Estimated Index of Refraction	Optically Measured Index of Refraction
0% DR-1	1.512	1.5
5% DR-1	1.602	1.61
10% DR-1	1.673	1.621

The results for the 5% PMMA/DR-1 samples were more unreliable than the 10% PMMA/DR-1 samples. One reason for this could be secondary reflections caused by the glass substrates. The 10% samples were slightly thicker (~1.2 μm compared to ~0.8 μm) than the 5% samples. The thicker samples helped reduce the chance of the secondary reflection and produced more precise data. Another factor could be impurities in the polymer. Due to the sensitive nature of the ellipsometer, any impurity could cause a change in thickness, which in turn would cause a change in the index of refraction. This could also lead to the slightly elevated average of the measured index of refraction.

Electro-Optic Effect

The EO effect was measured using a modified version of the Michelson interferometer. The modified version can be seen in Fig. **4.15**. One of the major modifications from the original Michelson interferometer was the addition of a piezo-driven mirror for the reference arm of the interferometer. This created a scanning

Michelson interferometer. A scanning interferometer automatically generates several λ/4 optically biased measurement positions that makes continuous measurements possible. The scanning frequency was much smaller than the frequency at which the EO measurement was taken. Also, a polarizer was added to the light source. The addition of the polarizer filtered the x- or y-components of the electric field from the light source. This was important to help create the proper condition for both the transverse and longitudinal EO measurement.

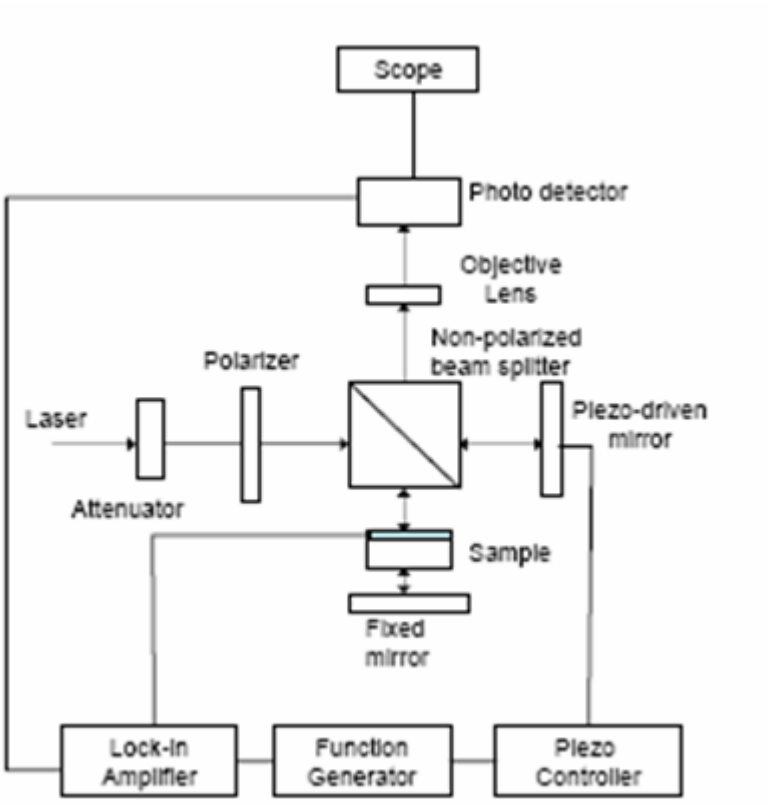

Fig. **4.15**: Modified Michelson interferometer setup.

The data from the Michelson interferometer was collected using a lock-in technique. The lock-in technique employs a lock-in amplifier to extract the output signal from the interferometer. A lock-in amplifier is a device that can extract a signal with a known frequency from a noisy environment. This is done by frequency mixing which converts the amplitude and phase of the signal into a dc voltage. Any frequency that is not the required frequency will be attenuated. This method was required due to the sensitive nature of the EO effect measurements. Typically the linear EO effect is on order of picometers per volt and the quadratic EO effect is on the order of 10^{-14} m^2/V^2, so the presence of any noise would cause error in the measurement. For this experiment, an SRS SR830 DSP lock-in amplifier was used.

The SRS SR830 was connected to a computer to control the system and collect the data automatically. A LabView computer program was written to gather the data. The output of the system was connected to both the lock-in and an oscilloscope to gather the peak-to-peak voltage of the system. The electric field was applied with the output capability of the SRS SR830 as well as the harmonic of the output. The piezo-driven mirror was driven with a function generator. A 60 mW helium-neon laser with a wavelength of 632.8 nm was used as the light source.

Before placing the samples in the interferometer setup, 0.001" diameter silver wires were attached to three of the platinum top electrodes using silver conductive epoxy. One wire was attached to an electrode on the base ITO layer, and the other two were attached to consecutive electrodes on the polymers. This configuration permitted for measuring both the longitudinal and transversal measurements. A diagram for the different EO measure configurations can be seen in Fig. **4.16**. After the samples were

wired, they were placed in sample arm of the experimental setup. Using the SR830, a voltage was applied to the sample starting at 0.5 V in increments of 0.5 V up to 5 V. The peak-to-peak output voltage was then recorded from the oscilloscope after approximately 20 minutes. This was done so a large sample size could be taken and checked for contamination (both light and vibration) of the data.

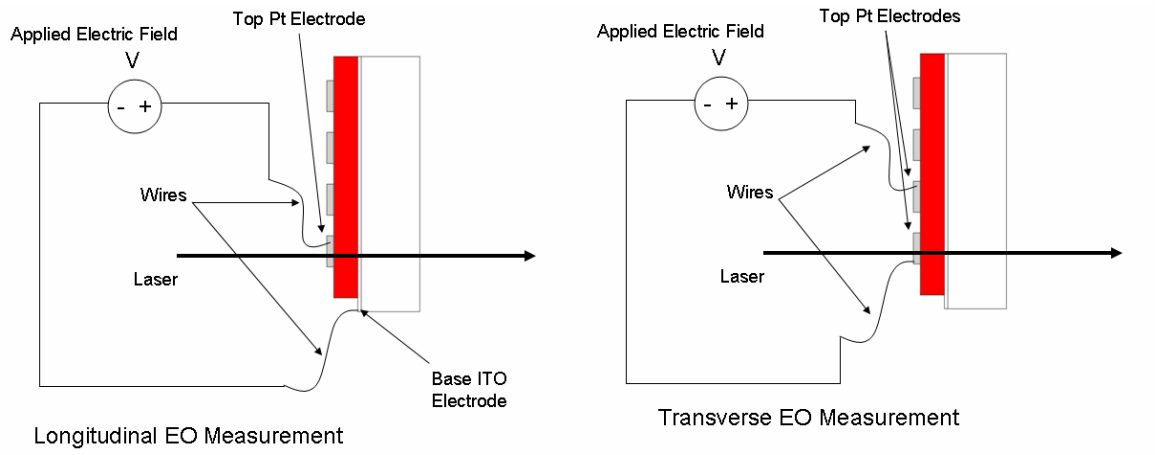

Fig. **4.16**: Diagram of the two different EO measurement setups used. (Right) Longitudinal EO measurement setup where on wire attached to the base ITO electrode and the other is attached to a top electrode, creating an electric field in the same directions as the laser. (Left) Transverse EO measurement setup where the wires are attached on adjacent top electrodes, creating an electric field in the perpendicular direction of the laser.

A problem arose during the measuring of the EO effect; the effect was too weak for any EO effect to be discernable. This was noticed when the applied electric field was increased and the peak-to-peak output voltage did not significant increase. The recorded data was very weak little or no phase and amplitude change was noticed. This could possible be attributed to the thickness of the polymer film. If the film was not thick enough, a detectable change in the amplitude and phase, $\varphi = \frac{2\pi \cdot \Delta n \cdot l}{\lambda}$, of the setup

would not have been possible. Using Eq. **3.2** and estimating the value of K to be 60×10^{-14} m^2/V^2 (the value commonly reported for $LiNbO_3$), it would take a field of approximately 1×10^{12} V/m to produce a phase change of π radians for a sample 1 μm thick (the average thickness of the polymer samples). A field this large would be impractical to generate even in a laboratory setting and would most likely cause sample breakdown prematurely.

Chapter 5

Conclusion and Future Work

Conclusion

The purpose of this research was to explore the thin film synthesis and the dielectric and optical characteristics of a nonlinear polymer solution. The polymer was tested to see if the proper characteristics were present to possibly be used in high frequency modulators. A guest-host polymer system was chosen, with PMMA being the host polymer and DR-1 being the nonlinear guest chromophore. Three solutions with different concentrations (0%, 5% and 10% DR-1) of the chromophore were prepared. These three concentrations were chosen due to reports that the chromophore overload with larger concentrations in the guest-host systems. Thin film samples of uniform composition, thickness, and smoothness were successfully fabricated for all three concentrations by spin coating. The relative dielectric constant and loss factor were measured and found to be in good agreement with the reported values. The plasticizing effect that the chromophore had on the PMMA was observed by measuring the temperature dependent relative dielectric constant and loss factor. The loss peaks, especially the α peak, shift to lower temperature with the greater concentration of the DR-1. The activation energies for the α and β relaxations were calculated by using the Arrhenius equation, which also indicated that the T_g decrease with higher concentration of DR-1.

A voltage was applied to the sample in an attempt to align the dipole moments of the chromophore. Breakdown in the film (the capacitance and loss shorting) was a problem with the thinner samples. Any motion of the dipoles in the chromophore that would have taken place when the voltage was applied did not become permanent at the poling conditions. A P-E measurement was taken and showed a weak nonlinear response that become more noticeable at elevated electric fields. Also, the biased dielectric measurement was determined by finding the slope of the linear section of the P-E graph.

The optical indexes of refraction of the samples at room temperature and at 632.8 nm were measured with an ellipsometer. The index value obtained by ellipsometry and estimated from dielectric measurement yielded good agreement. A modified version of the Michelson interferometer was setup for measuring the EO effect of the samples. The interferometer was altered to permit the measurements to be collected autonomously using a LabView computer program. The EO effect measurement was attempted with the samples, but no discernable effect was observed. This can be attributed to two main factors. The first reason was the fact that there was no appreciable nonlinearity after applying the voltage to the samples. The second factor can be attributed to polymer layer being too thin to properly generate a measurable change in phase under a feasible applied electric field. A thicker sample would be able to properly output a discernable change in phase, which in turn would produce a large EO effect.

Overall, it can be determined that the guest-host polymer system used in its present form would not be ideal for replacement of current EO materials available. However, the dielectric measurements showed promise for future investigations of different polymer families. The low frequency dielectric measurements were

extrapolated to the optical frequency. The methodology used in this experiment provided for a close estimate of the optical frequency measurements and could used to test other families of polymers. Effective poling method or optimization of the film to significantly improve its breakdown behavior may be keys to explore the full optical potential of the material.

Future Work

One important aspect of this experiment that could be altered to improve the measurements would be using a polymer that has a higher T_g for the guest-host system while maintaining thermal stability. By increasing the T_g of the polymer, a higher temperature can be applied to the sample. An increased temperature would then allow the dipole moments of the chromophore to move around freely with a smaller applied electric field, thus creating the opportunity for relatively larger NLO activity. Studies by Yesodha et al. [**3**] have recently been done using polyimides that exhibit a T_g of 220 °C. Also, various crosslinking techniques have been introduced to help improve the thermal properties and increase the concentration of the chromophore for current guest-host systems. A higher concentration of chromophore will increase the overall NLO activity in the polymer system. A properly crosslinking setup can be seen in Claude [**20**].

Another suggestion for improvement would be increasing the thickness of the polymer layer in the sample if the device application calls for longitudinal EO effect. An increase in the thickness would directly affect the longitudinal EO effect of the sample. As previously stated, the current sample structure did not permit for a sufficient phase

difference to be generated for the existing optical measurement. By increasing the thickness of the polymer, the applied electric field required to generate a phase difference would in turn decrease. An increase in thickness may affect the tunability of the samples (by requiring a large voltage to be used), so testing would be required to find a balance between the two. The thin film configuration is advantageous for transverse EO effect in waveguide form.

A different optical measurement technique could also be applied to help gather the required optical data. A scanning Mach-Zehnder interferometer (such as the one presented in Lu et al [**21**]) using only a single pass through the sample, reducing the amount of attenuation and absorption caused by the sample. This could decrease the amount of signal that would need to be applied to generate an EO effect. Another technique is the two-beam polarization interferometer setup suggested by Spirin et al [**22**] which is currently being used to measure the quadric EO coefficient in lead zirconate titanate thin films.

Bibliography

1. Haxha, S.; Rahman, B. M. A.; Grattan, K. T. V. "Bandwidth estimation for ultra-high speed lithium niobate modulators", *Applied Optics*, **42**, 2674-2682.

2. Dina, R.; Parker, T. C.; Huang, D.; Jin, D. L.; Koeing, M. "Systematic Study of Polymer Wideband Optical Modulators: Transition from Intrinsic Material Characteristics to Device Performance", Proceedings of SPIE, **5724** (2005), 88-95.

3. Yesodha, S. K.; Pillai, C. K.; Tsutsumi, N. "Stable polymeric materials for nonlinear optics: a review based on azobenzene systems", *Prog. Polym. Sci.*, **29**, 45-74.

4. Huang, D.; Parker, T.; Guan, H. W.; Cong, S.; Jin, D.; Dinu, R.; et al. "Development of Side-Chain NLO Polymer Materials with High Electro-Optic Activity and Long-Term Stability", Proceedings of SPIE, **5624** (2005), 172-181.

5. Kang, J. W.; Kim, T. D.; Luo, J.; Haller, M.; Jen, A. K. Y. "Very large electro-optic coefficients from *in situ* generated side-chain nonlinear optical polymers", *Appl. Phys. Lett.*, **87** (2005), 071109.

6. Boyd, R. W. *Nonlinear Optics*. 3rd Ed., Academic Press, New York, 2008.

7. Yariv, A. *Optical Electronics in Modern Communications*. 5th Ed., Oxford University Press, New York, 1997.

8. Lei, D.; Runt. J.; Safari, A.; Newnham, R. E. "Dielectric Properties of Azo Dye-Poly(methyl methacrylate) Mixtures". *Macromolecules*, **20** (1987), 1797-1801.

9. Balkrishnan, M.; Diemeerm M. B. J.; Driessen, A.; Freccini, M.; Verboom, W.; Reinhoudt, D. N.; Leinse, A. "Electro-optic polymers for high speed modulators", Proceedings Symposium IEEE/LEOS Benelux Chapter. 2005, 313-316.

10. Bernini, U.; Russo, P.; Mallinconico, M.; Martuscelli, E.; Volpe, M. G.; Mormile, P. "Temperature dependent optical properties of a synthesis blend of poly(methyl methacrylate) and vinyl rubber", *J. Mat. Sci.*. **28** (1993), 6399-6403.

11. Pretre, P.; Wu, L.-M.; Knoesen, A.; Swalen, J. D. "Optical properties of nonlinear optical polymers: a method for calculation", *J. Opt. Soc. Am. B.,* **15** (1998), 359-368.

12. Fedosov, S. N.; Segeeva, A. E. "Corona poling of ferroelectric and nonlinear optical polymers", *Moldavian Journal of Physical Sciences*, **N2** (2002), 28-31.

13. Giacometti, J. A.; Fedosov, S.; Costa, M. M. "Corona Charging of Polymers: Recent Advances on Constant Current Charging", *Brazilian Journal of Phys.*, **29** (1999), 269-279.

14. Pliška, T.; Meier, J.; Eckau, A.; Ricci, V.; Le Duff, A. C.; Canva, M.; et al. "Relative electrical resistivities and poling of nonlinear optical polmeric waveguides", *Appl. Phys. Lett.*, **76** (2000), 265-267.

15. Yue, Z. Z.; An, D.; Chen, R. T.; Tang, S. "1000 V/μm pulsed poling technique for photolime-gel electro-optic polymer with room-temperature repoling feature", *Appl. Phys. Lett.*, **72** (1998), 26, 3420-3421.

16. Jonscher, A. K. *Dielectric Relaxation in Solids*. Chelsea Dielectrics Press, London, 1983.

17. Vetrov, A. A.; Lipovskii, A. A.; Tagantsev, D. K. "A Highly Sensitive Technique for Measurements of the Kerr Electrooptic Coefficient in Glasses and Glass Ceramics", *Instruments and Experimental Techniques*. **45** (2002), 4, 550-554.

18. Bergman, R.; Alvarez, F.; Alegria, A.; Colmenero, J. "Dielectric relaxation of PMMA revisited", *Journal of Non-Crystalline Solids.* **235-237** (1998), 580-583.

19. Singer, K. D.; Kuzyk, M. G.; Holland, W. R.; Sohn, J. E.; Lalama, S. J.; Comizzoli, R. B.; et al. "Electro-optic phase modulation and optical second-harmonic generation in corona-poled polymer films", *Appl. Phys. Lett.* **53** (1988), 1800-1802.

20. Claude, Jason W. "Application of a Disperse Red One – Poly(methyl methacrylate) Non-Linear Optical Polymer For an All Fiber Tunable Filter", MS Thesis, The Pennsylvania State University, 2006.

21. Lu, Y.; Cheng, Z.-Y.; Park, S.-E.; Liu, S.-F.; Zhang, Q. "Linear Electro-optic Effect of $0.88Pb(Zn_{1/3}Nb_{2/3})O_3$-$0.12PbTiO_3$ Single Crystal", *Jpn. J. Appl. Phys.* **39** (2000), 141-145.

22. Spirin, V. V.; Lee, C.; No, K. "Measurement of the quadratic electrooptic coefficient of lead zirconatre titanate thin film by a two-beam polarization interferometer", *Optics Communications*, **158** (1998), 239-249.

Appendix A

Fabrication Parameters

A trial-and-error method was used to establish the optimal parameters for fabricating the thin film polymer samples. These parameters include the percent dry weight (combined weight of PMMA and DR-1), the percent DR-1 concentration, and the spin coating speed and time. Table **A.1** is a list of the percent dry weight and percent DR-1 tested to determine the most advantageous combination for spin coating. It was determined that 10% dry weight was the best choice and 5% and 10% DR-1 concentration produced good quality films for measurement. A 0% DR-1 concentration (pure PMMA) mixture was also produced to compare with the other combinations. Table **A.2** consists of list of different speeds used in spin coating. A spin time of 2 minutes was used to help increase the amount of solvent dissolved in the spin coating process. A problem that occurred with the slower speed was that the solution would not spin out onto the entire substrate, leaving some areas not covered with the polymer thin film. Also, the polymer would collect at the edges of the substrate causing the thickness of the film to vary greatly throughout the sample. The fastest speed (1000 RPM) would leave certain areas with little or no film. This made the thickness of the film fluctuate greatly. The most favorable spin speed was found to be 600 RPM. This speed created the most consistent film.

Table **A.1**: Percent DR-1 concentration and overall percent of dry weight trails. By testing the listed conditions it was determined that 10% overall dry weight was the optimal value and 5% and 10% DR-1 concentration produced good quality films.

Percent DR-1	Overall Percent of Dry Weight	Result
10%	15%	Thick, difficult to use with spin coating, leaves bubbles in film
10%	5%	Thin, doesn't completely "stick" to substrate, leaves bubbles and streaks in film
5%	10%	Mixes and spins properly, lighter shade of red
10%	10%	Mixes and spins properly, darker shade of red
15%	10%	DR-1 not completely dissolved, particulates in film

Table **A.2**: Spin coating speeds tested to produce highest quality polymer thin film. It was determined that 600 RPM created the highest quality film. Spinning time for all runs was 2 minutes.

Spin Speed (RPM)	Consistent?	Average Thickness	Comments
100	No	-	Didn't properly spin, areas of substrate not covered at all
250	No	-	Didn't properly spin, areas of substrate not covered at all
400	No	-	Polymer collected at edges, approx. twice as thick at edges compared to center
500	Yes	1.5 μm	Some polymer collected at edges, not as significant as slower speeds, small amount of "pinholes"
600	Yes	1 μm	Highest quality results, little or no "pinholes"
750	Yes	0.8 μm	Some areas thinner than other, medium amount of "pinholes"
1000	No	-	Areas of substrate contain little to no polymer, inconsistent thickness